

SYSTEM IDENTIFICATION OF FEI-TSUI ARCH DAM FROM FORCED VIBRATION AND SEISMIC RESPONSE DATA

CHIN-HSIUNG LOH

*Professor and Director, National Taiwan University,
Civil Engineering Department and National Centre for Research on
Earthquake Engineering, Taipei, Taiwan 10617, ROC*

TSU-CHIU WU

*Research Associate, National S&T Program for Hazard Mitigation Office,
National Taiwan University, Taipei, Taiwan, ROC*

Received 4 September 1998

Revised 25 February 2000

Accepted 3 May 2000

This paper presents the experimental investigation of the Fei-Tsui arch dam using the forced vibration test and its seismic response data. A forced vibration test was conducted on Fei-Tsui dam, this study presents the identified dynamic properties of the dam from these test data. For the identification of dam properties from seismic response data, in order to consider the nonuniform excitation of the seismic input and to describe the global behavior of the dam, the multiple input/multiple output discrete-time ARX model with least square estimation is applied to identify the dynamic characteristics of the dam. The system modal frequency, damping ratio and frequency response function are identified from both the forced vibration and seismic response data. To verify the accuracy of the identification result, comparison between discrete-time ARX model and a frequency domain conditioned spectral analysis was made. Finally, the spatial variation of ground motion across the free-field canyon surface is also studied.

1. Introduction

In recent years, system identification techniques have been widely adopted to estimate dynamic properties of building structures. However, these techniques have scarcely been used on an actual seismic response of a dam-reservoir system. There are two major reasons for this: there have been very few observations undertaken, especially the intensive strong motion array instrumentation on dam response during earthquake, and also too many uncertainties on the observations, especially the effects of reservoir water. For the second reason, when a dam-reservoir system is subjected to earthquake, the hydrodynamic pressures and the deformation of the dam interact with each other. In general, the behaviour of the dam-reservoir system during earthquake loading is a coupled dynamic interaction problem. However, it is believed that post-earthquake seismic safety assessment of the dam based on the seismic records is important to the dam engineers.

Application of identification techniques to the experimental data and the recorded seismic response of the building had been studied based on the discrete-time linear filter approach [Safak, 1989a, 1989b; Bhonem *et al.*, 1991; Loh *et al.*, 1995]. In contrast, identification on the seismic response data of dam is much more complex than the building structures. However, seismic records provided one of the few source of information on the dynamic characteristics of the dam-reservoir interaction problem. Besides the study on the seismic response data of dam, another method to study the dynamic characteristics of an arch dam is to conduct steady state force vibration tests on existing dam [Abdul-Ghaffar and Scott, 1981; Clough *et al.*, 1984; Duron and Hall, 1986]. The frequency response curves obtained from these tests can be utilised to find the natural frequency and damping ratios. Based on the nonclassical modal synthesis formulation a method is also developed for the interpretation of frequency test results of arch dam [Mau and Ghia, 1988; Dinum *et al.*, 1982].

Before the seismic event occurred, the forced vibration test is one of the reliable experimental approach to obtain the dynamic properties of a dam. A forced vibration test was conducted on Fei-Tsui dam, this study presents the test results and also the identified dynamic properties of the dam from these test data. A well-instrumented strong-motion array on the Fei-Tsui arch dam (Taiwan) was established in 1991. Some seismic response data were collected from this dam. One of main purpose of this paper is to use the system identification techniques to study the dynamic characteristics of the dam from seismic response data. In order to consider the nonuniform excitation of the dam abutment and describe the global behavior of the dam body, the multiple input/multiple output discrete-time ARX model with least square estimation is selected for the identification. To verify the accuracy of the identification results of the ARX model, comparison between the discrete-time ARX model and a frequency domain conditioned spectral analysis was made. Finally, the spatial variation of ground motion across the free field canyon surface is also studied.

2. Description of the Fei-Tsui Dam

Built in April 1987, the Fei-Tsui concrete arch dam is 122.5 m high and 510 m long, and is constructed with a layout of three-centred double curvature with variable thickness. The dam was constructed in a way that dam body was divided vertically into 29 strips and each of the strip is about 17.5 m wide. Water seal is installed between any two adjacent strips. Because of the importance of Fei-Tsui arch dam, a well instrumented strong-motion array (see Fig. 1) was established on the dam in 1991 in order to monitor its seismic behaviour. The strong motion instrument project of Fei-Tsui dam includes 11 SSA-1 type (3-components) strong motion seismometers on the dam body. Five of them are along the dam foundation, three of them are at the crest level and three of them are near the center of the dam at a level of 115 m. About 400 meters away (downstream side) there are

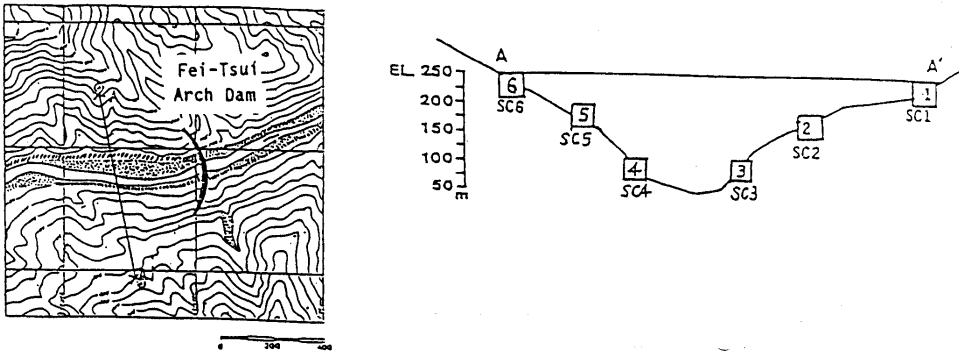


Fig. 1(a). Location of accelerometers along the canyon (400 m downstream from the dam site.)

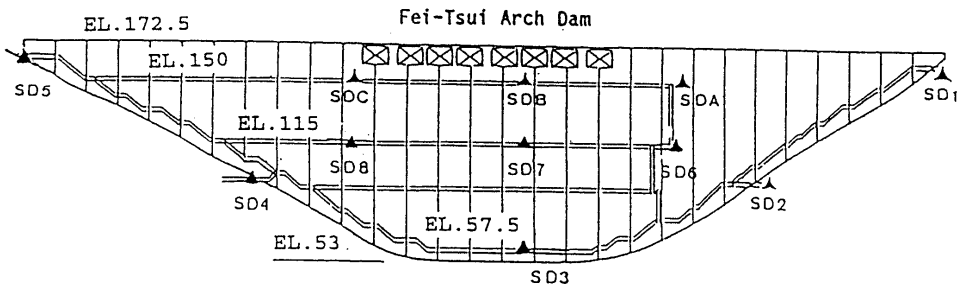


Fig. 1(b). Location of accelerometers at Fei-Tsui arch dam.

six accelerometers along the canyon surface to detect the free field seismic ground motion.

Since the operation of strong motion array, some seismic records have been collected from the dam as well as the free field ground motion along the canyon. Records are all in digital signal with a sampling rate of 0.005 second per point. Table 1 lists the recorded earthquake catalog as well as the reservoir water level for each seismic event. Most of the recorded earthquakes have magnitude less than 6.0 and hypocenter distance greater than 34 km. The recorded maximum acceleration at station SDB (at the center of the crest level) and station SD3 (at the center of the dam toe level) from the recorded seismic events is also shown in Table 2. Most of the recorded accelerations are very small (with magnitude 10^{-3} g level) except the 1994-6-5 earthquake with 32.37 gal of maximum acceleration at station SDB in upstream-downstream direction (East-West direction). Preliminary analysis of the seismic response data of the dam had been studied [Loh and Wu, 1996]. The Chi-Chi earthquake that occurred in Taiwan on September 21, 1999, the epicenter of this earthquake is at 23.85°N and 120.78°E (see Fig. 2) with magnitude 7.3 and focal depth of 7.5 km. The Chi-Chi earthquake triggered the recording system of Fei-Tsui dam (water level is 151.7 km during this earthquake), but triggered only a few of seismometers along the canyon surface (because of the problem

Table 1. Recorded earthquake catalogue at the Fei-Tsui Dam strong motion array.

Earthquake		M_L	Depth (km)	Distance (km)	Water level ^a (m)
1992-4-19	N 23° 54.43'	5.6	8.07	108	163.66
	E 121° 34.47'				
1992-4-20	N 24° 27.05'	4.9	8.80	102	163.61
	E 120° 42.86'				
1992-9-1	N 23° 41.98'	5.5	50.96	133	160.95
	E 121° 46.48'				
1992-9-28	N 23° 52.97'	5.9	17.58	236	167.57
	E 121° 46.35'				
1994-5-24	N 23° 49.60'	6.6	4.5	120	155.46
	E 122° 36.20'				
1994-6-5	N 24° 27.74'	6.2	5.30	43	155.61
	E 121° 50.26'				
1995-2-23	N 24° 12.22'	5.7	21.7	74	168.16
	E 121° 41.22'				
1995-6-25	N 24° 36.37'	6.0	39.9	34	158.67
	E 121° 40.11'				
1995-12-1	N 24° 36.36'	5.7	45.07	37	156.42
	E 121° 38.56'				

^aWater level: defined as the above sea level (the bottom of the dam is at a level of 52 m).

Table 2. Recorded maximum acceleration (gal) at station SDB and station SD3 from nine seismic events of SMART-C&D array.

Fei-Tsui dam	Station: SDB			Station: SD3		
	EW	NS	VT	EW	NS	VT
1992-4-19	5.39	1.76	1.12	0.71	0.70	0.95
1992-4-20	10.18	1.49	1.28	0.74	0.99	0.58
1992-9-1	16.50	2.17	1.91	1.66	1.21	1.19
1992-9-28	7.75	2.07	2.92	1.28	1.44	1.35
1994-5-24	13.00	2.30	1.44	2.33	1.42	1.18
1994-6-5	32.37	12.44	10.36	8.14	6.95	5.28
1995-2-23	7.46	2.24	2.05	1.91	1.71	0.87
1995-6-25	31.21	9.41	8.30	6.46	5.55	4.45
1995-12-1	5.48	1.13	1.51	1.54	1.19	0.97

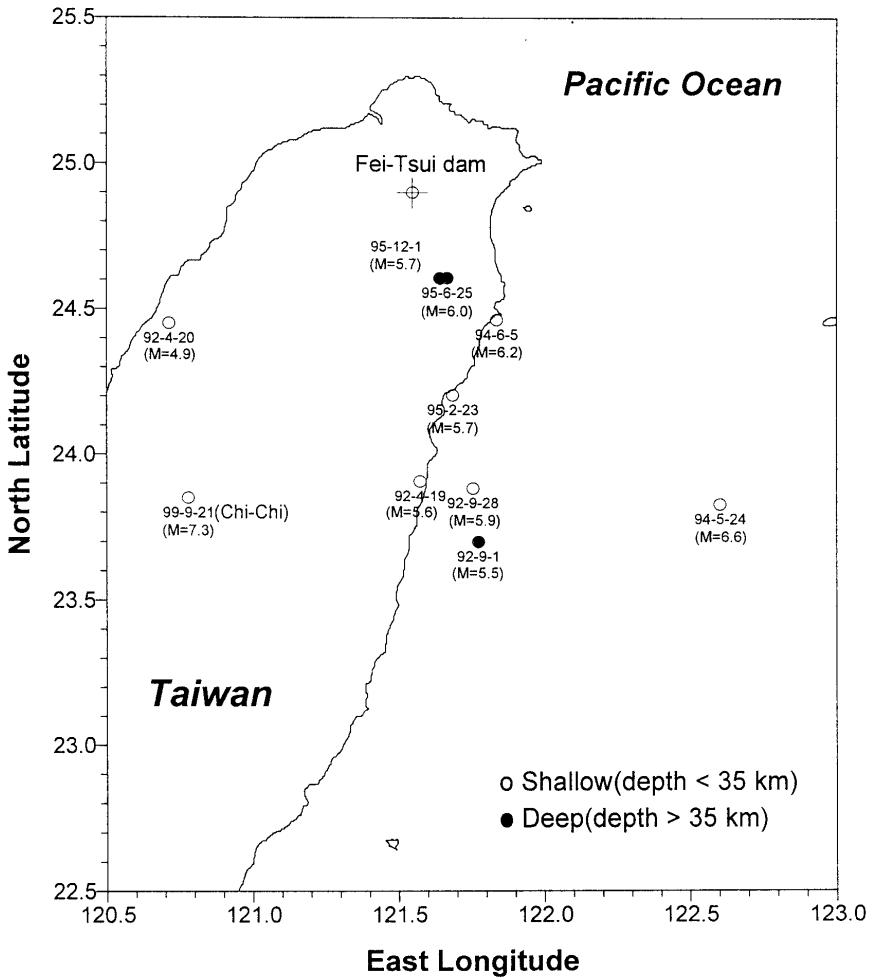


Fig. 2. Location of Fei-Tsui dam (epicentres of ten earthquakes recorded by Fei-Tsui dam).

of battery system). Some of the recorded acceleration and corresponding Fourier amplitude are shown in Fig. 3, the maximum peak acceleration response at the dam crest is 136.51 gal at station SDB (east-west direction). This paper applied the identification techniques to investigate the dynamic characteristics of the dam from the seismic datas, and comparison the identified result between low level seismic excitation (earthquake events as Table 1 list) and strong motion excitation (the Chi-Chi earthquake) was made.

Forced Vibration Test

The method of forced vibration test can be a reliable experimental approach to obtain the frequency response functions of a large scale civil engineering structure,

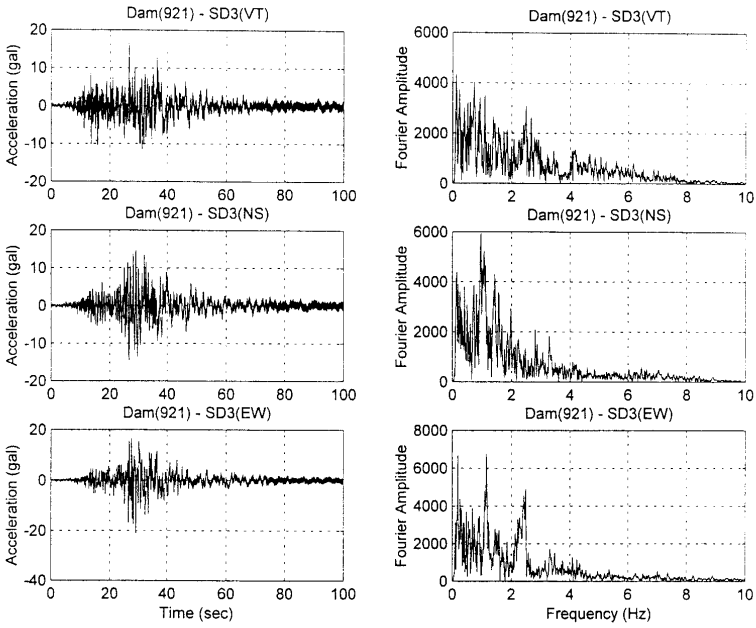


Fig. 3(a). Recorded acceleration and the corresponding Fourier amplitude at station SD3 for earthquake of 21 September 1999.

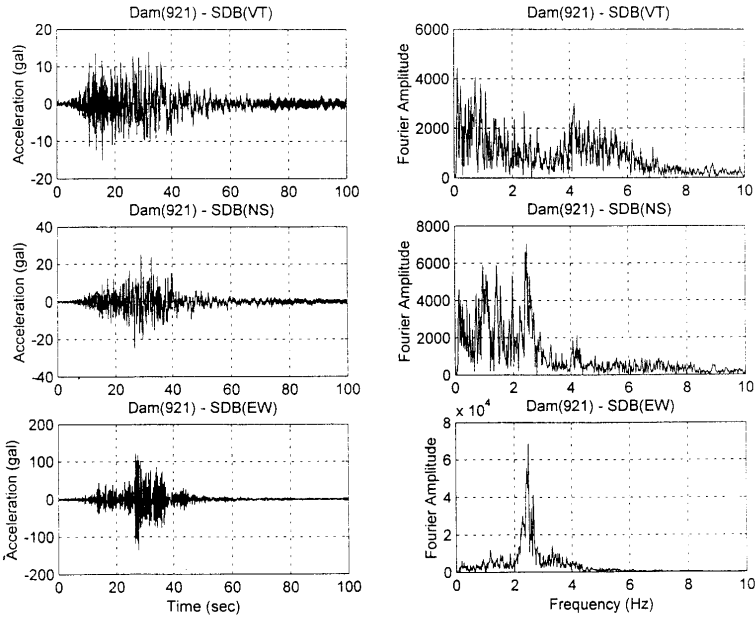


Fig. 3(b). Recorded acceleration and the corresponding Fourier amplitude at station SDB for earthquake of 21 September 1999.

such as a dam [Mau and Wong, 1989]. The structure is excited step by step by a series of sinusoidal forces of known magnitudes and frequencies. At each excitation frequency the steady state response is recorded for further analysis. In this study, the forced vibration method was applied to Fei-Tsui arch dam at a water level of 169.1 m in the reservoir. A rotating eccentric mass shaker system capable of producing a 5-ton maximum sinusoidal force at a rotating speed of 4.5 Hz was mounted on the dam crest. To avoid the effect of dam spillway, the shaker was located about one-third of the crest length measured from its left abutment as shown in Fig. 1(b). Due to this arrangement of the shaker, it was possible to excite both symmetric and antisymmetric modes of the dam. The responses of the dam were measured by velocity sensors at 10 stations located along the crest with an interval of 50 meters. For each excitation frequency, 20 cycle time history data of dam response were recorded. By using a least square fitting scheme, the recorded time data were forced to fit the following harmonic equation

$$v_i(t) = C_1 \cos 2\pi ft + C_2 \sin 2\pi ft \quad (1)$$

where $v_i(t)$ is the velocity measurement at the i th station, f is the known excitation frequency and C_1 and C_2 are two constants which are determined by the regression scheme. The amplitude and phase of the dam response $v_i(t)$ at the frequency f can be computed from Eq. (1). The phase (in radian) indicates how much the occurrence time of maximum dam response lags behind that of the maximum excitation force. Figure 4 shows the frequency response functions of amplitudes and phases of Fei-Tsui dam at the 10 measurement locations (10 channels).

The measurement presented in the figures was taken at the upstream-downstream (E-W) direction, only. Since the excitation force produced by the eccentric mass shaker is proportional to the square of the excitation frequency, the amplitude curves in Fig. 4(a) have been normalised by dividing the maximum response with the excitation force. The resonant frequencies identified from these two peaks are around 2.26 Hz and 3.02 Hz, respectively. With the help of the frequency response functions of phase lags shown in Fig. 4(b), the mode shapes associated with the two resonant frequencies can be drawn as in Figs. 5(a) and 5(b), respectively. From the mode shapes, it is seen that the vibration mode at 2.26 Hz is an antisymmetric model; while the one at 3.02 Hz is a symmetric model. In Fig. 4, it is noted that due to the tremendous mass of dam-reservoir system, the response excited by the shaker force was normally kept at a very low level throughout the experiment, thus the time response data were easily contaminated by electric and ambient noise. The noise is more influential in determining the phase lags than in determining the amplitudes, so the jaggy curves can be seen in the phase functions in Fig. 4(b). In order to fully utilise the above frequency response functions and to extract more information about dynamic properties of the dam, in this study, two modal model were adopted to identify the modal frequencies and damping ratios.

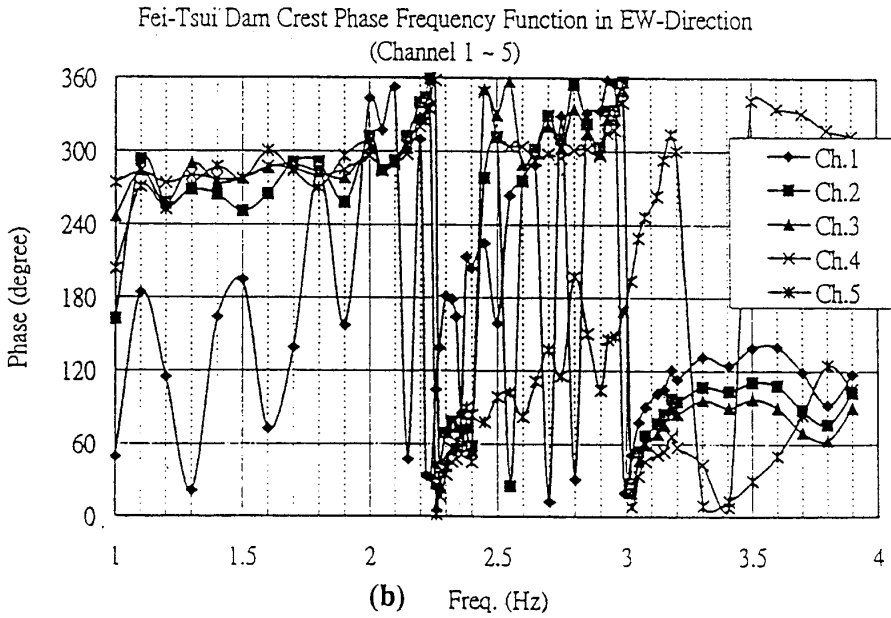
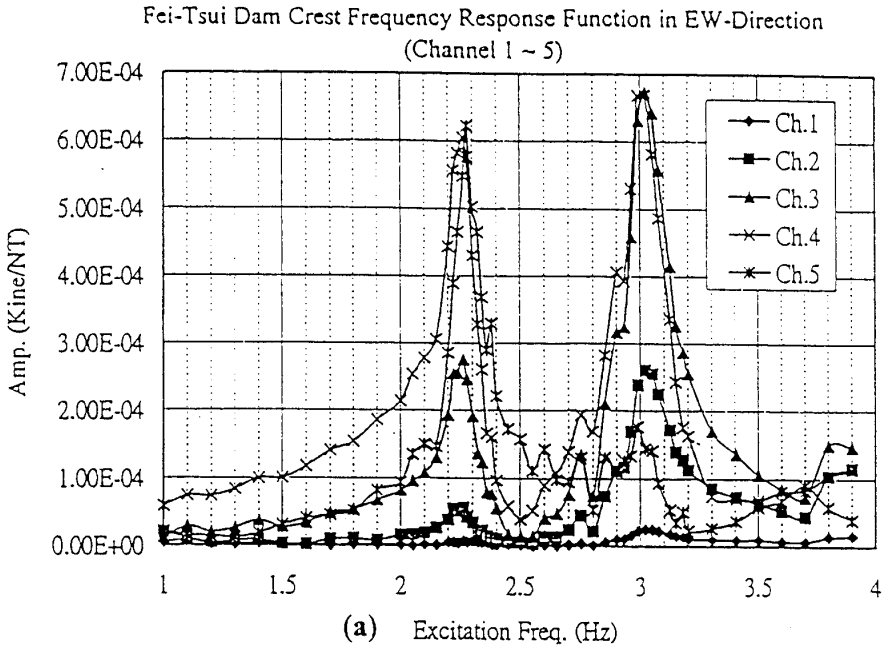
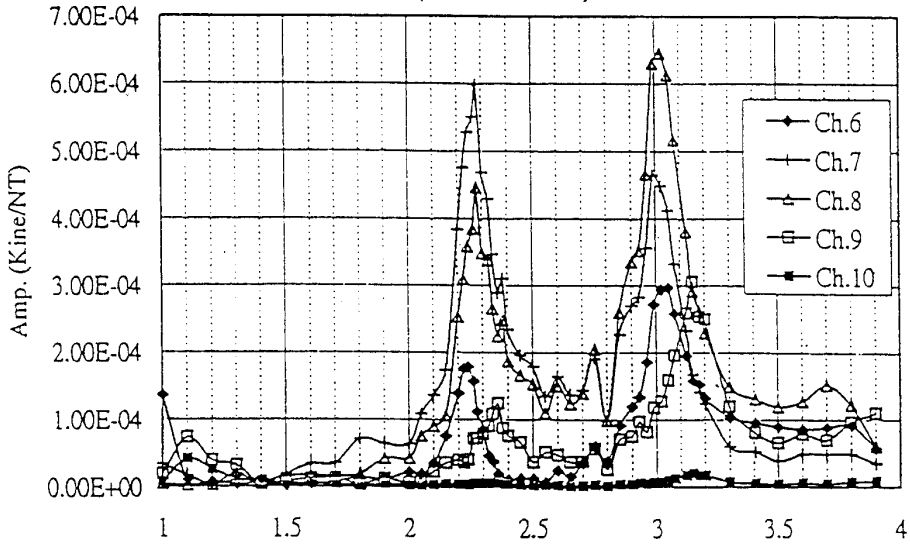


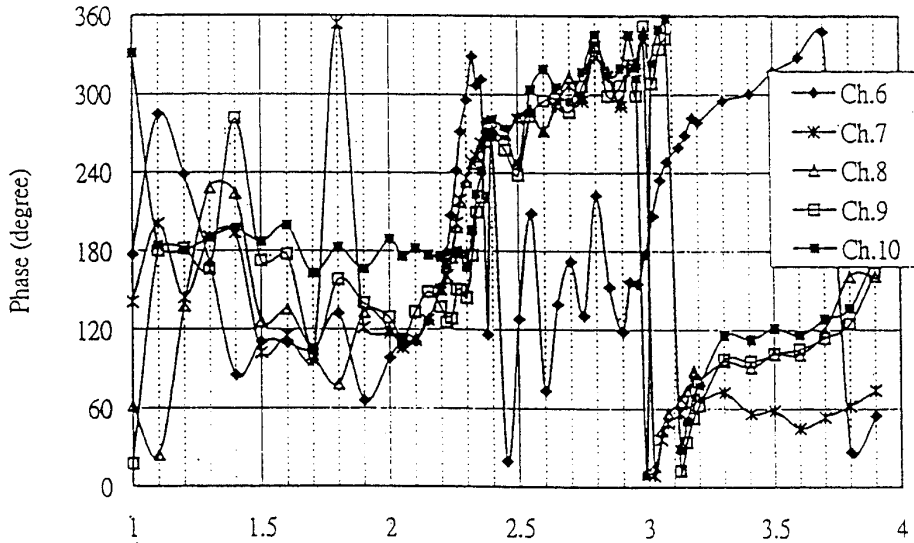
Fig. 4. Measured frequency response function and phase spectrum in radial direction from channel 1 to channel 10.

Fei-Tsui Dam Crest Frequency Response Function in EW-Direction
(Channel 6 ~ 10)



(a) Excitation Freq. (Hz)

Fei-Tsui Dam Crest Phase Frequency Response Function in EW-Direction
(Channel 6 ~ 10)



(b) Freq. (Hz)

Fig. 4. (Continued)

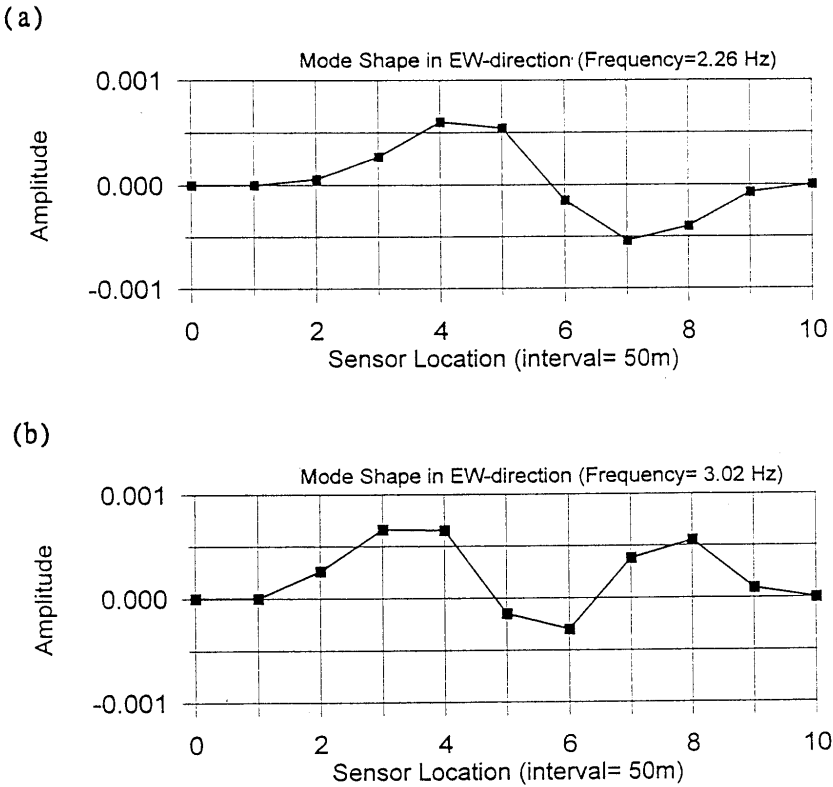


Fig. 5. Identified mode shapes along dam crest from forced vibration test: (a) mode shape at 2.26 Hz, (b) mode shape at 3.02 Hz.

2.1. A MDOF system with classical damping

Consider a n -degree-of-freedom system with classical damping under an external excitation $f(t)$ at the l th component. The j th modal equation can be written as

$$\ddot{q}_j + 2\omega_j \xi_j \dot{q}_j + \omega_j^2 q_j = \phi_{lj} f(t) \tag{2}$$

in which q_j is the j th mode of the generalised coordinate, and ϕ_j is the normalised model shape. The ω_j and ξ_j are modal frequency and damping ratio, respectively. For eccentric mass excitation mr was located at the l th component of the system, the $f(t)$ is $mr\omega^2 \sin \omega t$. Then the steady state acceleration of the i th component of the system is given by [Housner and Jennings, 1969]

$$\ddot{x}_i = \sum_{j=1}^n \frac{\phi_{ij} \phi_{lj} mr \omega^2 \left(\frac{\omega}{\omega_j}\right)^2 \sin(\omega t - \psi_j)}{\sqrt{\left[1 - \left(\frac{\omega}{\omega_j}\right)^2\right]^2 + \left(2\xi_j \frac{\omega}{\omega_j}\right)^2}} \tag{3}$$

where

$$\tan \psi_j = \frac{2\xi_j \left(\frac{\omega}{\omega_j}\right)}{1 - \left(\frac{\omega}{\omega_j}\right)^2}.$$

The effect of modal interference can be found from Eq. (3). Looking first at the response of the fundamental mode, Eq. (3) implies that $(\omega/\omega_j)^2$ is small for $j \geq 2$ when ω is near ω_1 . But for the second mode, with ω near ω_2 , the value of $(\omega/\omega_j)^2$ is small only for $j \geq 3$ and is relatively large for $j = 1$ with the result that the first mode response can be appreciable when ω is near ω_2 . The previous analysis can be extended to other high modes of modal interference. Based on Eq. (3) and incorporated with the measured frequency response functions and mode shapes, one can estimate the modal frequencies and damping ratios of the structure. The estimated modal damping and natural frequency are shown in Table 3.

Table 3. Comparison of the estimated modal frequencies and damping ratios using models with classical and non-classical damping.

Channel	Damping type	f_1 (Hz)	ξ_1 (%)	f_2 (Hz)	ξ_2 (%)	ξ_{12} (%)
1	Classical	2.29	0.83	3.04	1.95	0.00
	Non-classical	2.29	1.28	3.04	2.10	0.09
3	Classical	2.24	2.29	3.03	2.04	0.00
	Non-classical	2.24	2.34	3.03	2.09	0.40
5	Classical	2.28	1.97	2.99	2.03	0.00
	Non-classical	2.28	1.97	2.99	2.13	0.20
7	Classical	2.27	2.52	3.01	2.01	0.00
	Non-classical	2.27	2.52	3.01	2.06	0.35

2.2. A MDOF system with nonclassical damping

Different from classical damping case one may consider a n -degree-of-freedom system with nonclassical damping under harmonic excitation. The equation of motion associated with the i th modal coordinate is

$$\ddot{q}_i + d_{ii}\dot{q}_i + \omega_i^2 q_i + \sum_{\substack{j=1 \\ j \neq i}}^n d_{ij}\dot{q}_j = f_i u(t) \tag{4}$$

where d_{ij} ($i, j = 1, \dots, n$) are elements of the modal damping matrix, and f_i ($i = 1, \dots, n$) are nonzero constants. The scalar $u(t)$ is a harmonic function of unit amplitude. Applying the Laplace transform to Eq. (4), it can be rewritten as [Park and Ma, 1994]

$$Q_i(s) = \left\{ f_i / \left[s^2 + \left(d_{ii} + \sum_{\substack{j=1 \\ j \neq i}}^n d_{ij} \frac{Q_j(s)}{Q_i(s)} \right) s + \omega_i^2 \right] \right\} \cdot U(s) \tag{5}$$

where $Q_k(s)$ and $U(s)$ are the Laplace transforms of $q_k(t)$ and $u(t)$, respectively. Since the experimental data is measured in the frequency format, it is needed to convert Eq. (5) to the frequency domain. Consider a set of $Q_i(\omega)$ equation ($i = 1, \dots, n$) and the measured frequency response function, the modal frequencies and damping ratios can be estimated through regression analysis. As shown in Table 3, f_j and ξ_j ($j = 1, 2$) are the estimated modal frequencies and damping ratios, and ξ_{12} represents the estimated coupled damping effect. From the table, it is seen that results from the two different models are very consistent. This implies that the effect of nonclassical damping is negligible and the dam can be modelled as a system with classical damping during low level excitation.

3. Model of Linear Time-Invariant System

To analyse the seismic data of the dam the discrete-time method for system identification based on linear filtering and least square estimation are used. The multiple input/multiple output discrete-time ARX(MIMO) model was applied. A frequency domain conditioned spectral analysis (CSA) was also used to verify the multiple-support excitation for the prediction of seismic response of dam.

The most simple system model is the single input/single output ARX(SISO) model, using a difference equation to describe the input-output relationship

$$y(t) + a_1y(t - 1) + \dots + a_{n_a}y(t - n_a) = b_1u(t - 1) + \dots + b_{n_b}u(t - n_b) + e(t) \tag{6}$$

where a_i and b_j are the unknown parameters, n_a and n_b are the order of the output and input respectively, $e(t)$ is the white noise term.

If we introduce

$$A(q) = 1 + a_1q^{-1} + \dots + a_{n_a}q^{-n_a} \tag{7}$$

$$B(q) = b_1q^{-1} + \dots + b_{n_b}q^{-n_b} \tag{8}$$

where q^{-1} is a delay operator, i.e. $q^{-n}y(t) = y(t - n)$. Equation (6) can be rewritten as

$$A(q)y(t) = B(q)u(t) + e(t) \tag{9}$$

this model can be called as ARX(SISO) model, where AR refers to autoregression part, $A(q)y(t)$ and X refers to extra input $B(q)u(t)$. Equation (9) can be expressed as

$$y(t) = \phi^T(t)\theta + e(t) \tag{10}$$

where

$$\phi(t) = [-y(t-1), \dots, -y(t-n_a), u(t-1), \dots, u(t-n_b)]^T \tag{11}$$

$$\theta = [a_1, \dots, a_{n_a}, \dots, b_1, \dots, b_{n_b}]^T. \tag{12}$$

Equation (10) is a linear regression form, the unknown parameter vector θ can be obtained through the least square estimation method, once the parameters of the ARX model were identified, the system natural frequency and damping ratio of each structural mode can be estimated through the relation between discrete form of equation of motion (modal equation) and discrete-time ARX model.

The formulation of ARX model is very simple, It is easy to extend the model to multiple input/single output ARX(MISO) model, the input-output relationship can be described as

$$A(q)y(t) = B_1(q)u_1(t) + \dots + B_k(q)u_k(t) + e(t) \tag{13}$$

where $y(t)$ is single output and $u_j(t)$, $j = 1-K$, are the multiple inputs. Equation (13) can be rewritten as a linear regression form

$$y(t) = \Phi^T(t)\theta + e(t) \tag{14}$$

where

$$\begin{aligned} \Phi(t) = & [-y(t-1), \dots, -y(t-n_a), u_1(t), \dots, u_1(t-n_1) \\ & \times u_k(t-1), \dots, u_k(t-n_k)]^T \end{aligned} \tag{15}$$

$$\theta = [a_1, \dots, a_{n_a}, b_{11}, \dots, b_{n_11}, \dots, b_{1k}, \dots, b_{n_kk}]^T. \tag{16}$$

Similarly, the unknown parameter vector θ can be obtained by using least square estimation method, then system natural frequency and damping ratio are also estimated.

The formulation of the multiple input/multiple output ARX(MIMO) model is similar with Eq. (9). Consider the system having n_u inputs and n_y outputs, the discrete-time ARX(MIMO) model is given by

$$A(q)y(t) = B(q)u(t) + e(t) \tag{17}$$

but, here $A(q)$ is an $n_y \times n_y$ matrix whose entries are polynomials in the delay operator q^{-1} can be expressed as

$$A(q) = \begin{bmatrix} a_{11}(q) & a_{12}(q) & \dots & a_{1n_y}(q) \\ a_{21}(q) & a_{22}(q) & \dots & a_{2n_y}(q) \\ \vdots & \vdots & & \vdots \\ a_{n_y1}(q) & a_{n_y2}(q) & \dots & a_{n_y n_y}(q) \end{bmatrix} \tag{18}$$

where the entries a_{kj} are polynomials in the delay operator q^{-1} can be written as

$$a_{kj}(q) = \delta_{kj} + a_{kj}^1 q^{-1} + \dots + a_{kj}^{n_{a_{kj}}} q^{-n_{a_{kj}}}. \tag{19}$$

Here δ_{kj} is the Kronecker-delta. This polynomial describes how old values of output number j affect output number k . Similar, $B(q)$ is an $n_y \times n_u$ matrix and is given by

$$B(q) = \begin{bmatrix} b_{11}(q) & b_{12}(q) & \cdots & b_{1n_u}(q) \\ b_{21}(q) & b_{22}(q) & \cdots & a_{2n_u}(q) \\ \vdots & & & \vdots \\ b_{n_y1}(q) & b_{n_y2}(q) & \cdots & b_{n_y n_u}(q) \end{bmatrix} \tag{20}$$

with

$$b_{kj}(q) = b_{kj}^1 q^{-1} + \cdots + b_{kj}^{nb_{kj}} q^{-nb_{kj}}. \tag{21}$$

The generalised regression estimation method can be used to solve the unknown parameters [Ljung and Lennart, 1987].

The reason to use multiple inputs was examined by conditioned spectral analysis. Considered the multiple input and single output system, the input–output relationship was expressed as

$$Y(f) = \sum_{i=1}^n H_{iy}(f)U_i(f) + N \tag{22}$$

where n is the number of inputs, $H_{iy}(f)$ is the system frequency response function between input “ i ” and the output, and N represents uncorrelated output noise. For arbitrary input data $u_i(t)$, one can remove the correlated signals from the second signal $u_j(t)$ ($i \neq j$) [Bendat and Piersol, 1986]. Equation (22) can be replaced by the equivalent model with new uncorrelated inputs $U_1(f)$, $U_{2,1}(f)$ and $U_{3,21}(f)$ passing through new linear system $L_{1y}(f)$, $L_{2y}(f)$ and $L_{3y}(f)$. The input–output relationship became

$$Y(f) = \sum_{i=1}^n L_{iy}(f)U_{i,(i-1)!}(f) \tag{23}$$

where $U_{2,1}(f)$ is the residual record which the correlated part of signal $U_1(f)$ was removed from the signal $U_2(f)$. $U_{3,21}(f)$ is the residual record which the correlated part of $U_1(f)$ and $U_2(f)$ was removed from the signal $U_3(f)$. The system $L_{iy}(f)$ can be obtained using conditioned spectral density function and expressed as^{15,16}

$$L_{iy}(f) = \frac{G_{iy,(i-1)!}(f)}{G_{ii,(i-1)!}(f)}; \quad \text{for } i = 1 \cdots n \tag{24}$$

where $G_{iy,(i-1)!}(f)$ is the cross spectrum between $y(t)$ and $u_{i,(i-1)!}(t)$, and $G_{ii,(i-1)!}(f)$ is the autospectrum of input signal $u_{i,(i-1)!}(t)$. Once $L_{iy}(f)$ was estimated, a general procedure to determine the system frequency response function

$H_{iy}(f)$ from the L_{iy} system by working backwards can be developed. It is the important step to check whether the selected multiple inputs model is correct or not. At first, we define a partial coherence function and is given by

$$\gamma_{iy,j}^2 = \frac{|G_{iy,j}(f)|^2}{G_{ii,(i-1)}(f) \cdot G_{yy,(i-1)}(f)}; \quad \text{for } j \leq i - 1. \quad (25)$$

Partial coherence function is the magnitude that input $u_{i,j}$ contributes to output. In order to sum the coherence function for the entire multiple inputs model, cumulative coherence function, defined as various partial sums of these component coherence for a selected number of input terms, allows for inspection of the model for such combination of input terms. This can be written as

$$\gamma_{y:u}^2(f) = \gamma_{u_1y}^2(f) + \gamma_{u_2y}^2(f) + \dots \quad (26)$$

A good system model will be obtained at desired frequencies when the value of cumulative coherence function is close to unity. The cumulative coherence function can examine the input terms of the multiple input system. Figure 6 shows the cumulative coherence function by considering the transverse (east-west direction) motion of SDB station as output and SD3 station (EW and NS direction), SD4

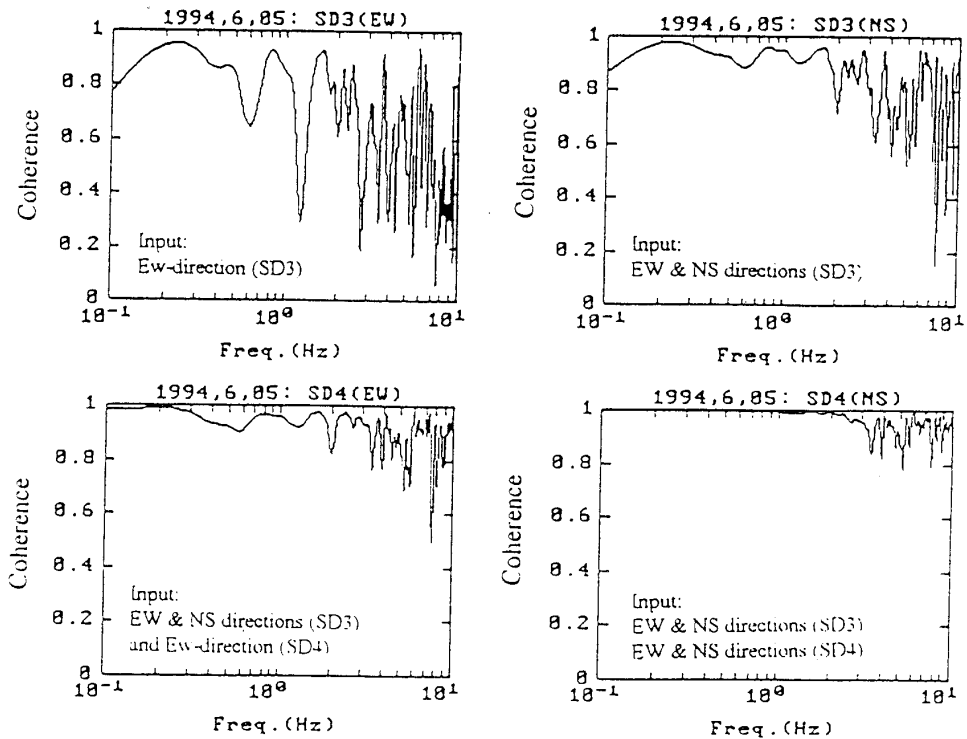


Fig. 6. Cumulative coherence function between inputs (SD3:EW,SD3:NS,SD4:EW, SD4:NS) and output (SDB:EW) for 1994-6-5 earthquake data.

station (EW and NS direction) as inputs, respectively. In this case, considering four inputs from abutment of the dam to estimate the output of SDB station can provide high coherence. Significant bias will occur if only single input motion from dam toe level was used to estimate the frequency response function. Based on the above discussion, a good system model is necessary to use the motion of SD3 (EW and NS direction), SD4 (EW and NS direction) as input to identify the dynamic behavior of the dam.

4. Results of Identification from Seismic Data

To identify the global behavior of the dam the response data of upstream-downstream direction (EW direction) of station SDB, SDC and SD7 are considered as outputs and motions along the abutments (5 stations) are considered as inputs. For the following analysis, the notation H (SDB:EW/SD3:EW) is used to describe the estimated frequency response between east–west input motion of station SD3 and east–west output motion of station SDB. System natural frequency, damping ratios and the identified frequency response function between each pair of input and output are discussed.

- (1) Discussion on the identified frequency response function H (SDB:EW/SD3:EW), H (SDB:EW/SD3:NS) and H (SDB:EW/SD3:VT) from different seismic events: The identified frequency response functions were shown in Fig. 7. The dominant frequency changes from event to event. This can be explained as a result of the changes in water level in the reservoir. The amplitude of H (SDB:EW/SD3:NS) at the dominant frequencies is greater than the amplitude of H (SDB:EW/SD3:EW). This means that the north–south component excitation at station SD3 will have a significant contribution to the response of the east–west component at station SDB.
- (2) Discussion on the identified frequency response function H (SDB:EW/SD3:EW), H (SDB:EW/SD4:EW) and H (SDB:EW/SD5:EW) from different seismic events: Fig. 8 shows the estimate frequency response function from same output (station SDB) but with different input (Station SD3, SD4 or SD5). It can be found that the amplitude of frequency response function is different with the different input during the same seismic event. It means that the multiple inputs model is needed to represent the nonuniform inputs from the abutment of the dam.
- (3) Discussion on the identified frequency response function H (SDB:EW/SD3:EW), H (SDC:EW/SD3:EW) and H (SD7:EW/SD3:EW) from different seismic events: Fig. 9 shows the estimated frequency response functions for different outputs. From Fig. 9, it was found that the estimated dominant frequency slight changes with the different output. The amplitude of estimated frequency response function also changes with the different output. Since the dam is a 3-dimensional large structure the dynamic of the dam is different from

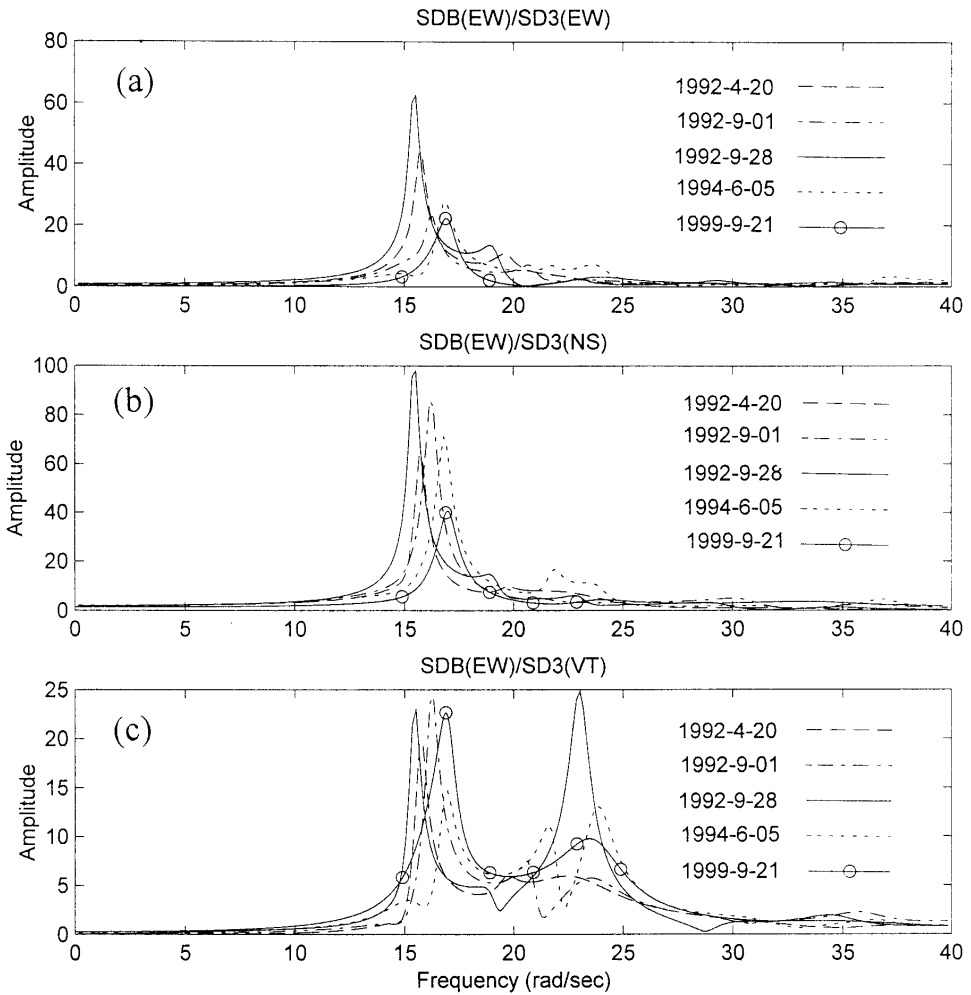


Fig. 7. Estimated frequency response functions by using multiple outputs (east-west direction of station SDB, SDC, SD7)/multiple inputs (all recorded motions along the abutment) ARX model for different events: (a) $H(SDB:EW/SD3:EW)$, (b) $H(SDB:EW/SD3:NS)$, (c) $H(SDB:EW/SD3:VT)$.

of a traditional building structure, it is necessary to use the multiple outputs model in the system identification.

- (4) Comparison on the identified dynamic characteristics of the dam from different seismic events: Fig. 10 shows the relationship between the identified modal frequency of the first two modes with respect to water levels. The results of discrete time ARX(MISO) model and conditioned spectral analysis (CSA) are also shown in the figure for comparison. From this figure, it is found that the dominant frequency of the dam-reservoir system decreases with the increase in reservoir water level, this can be explained as the effect of added mass

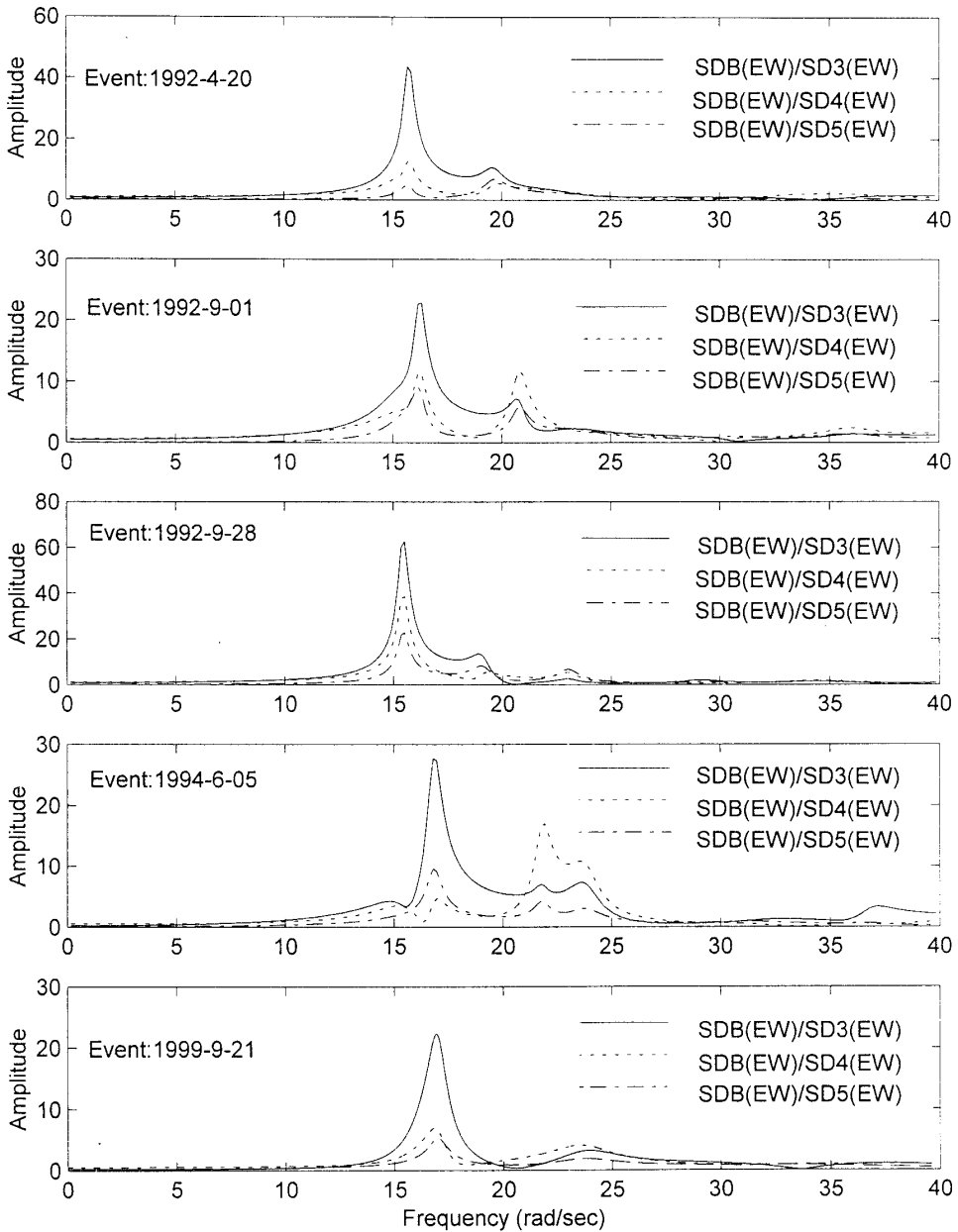


Fig. 8. Comparison on the identified $H(SDB:EW/SD3:EW)$, $H(SDB:EW/SD4:EW)$, and $H(SDB:EW/SD5:EW)$ from different seismic events.

from the water pressure. The identified regression line of ARX(MISO) model or ARX(MIMO) model maintain a straight line. But the identified natural frequencies from the forced vibration data are not very consistent with the results

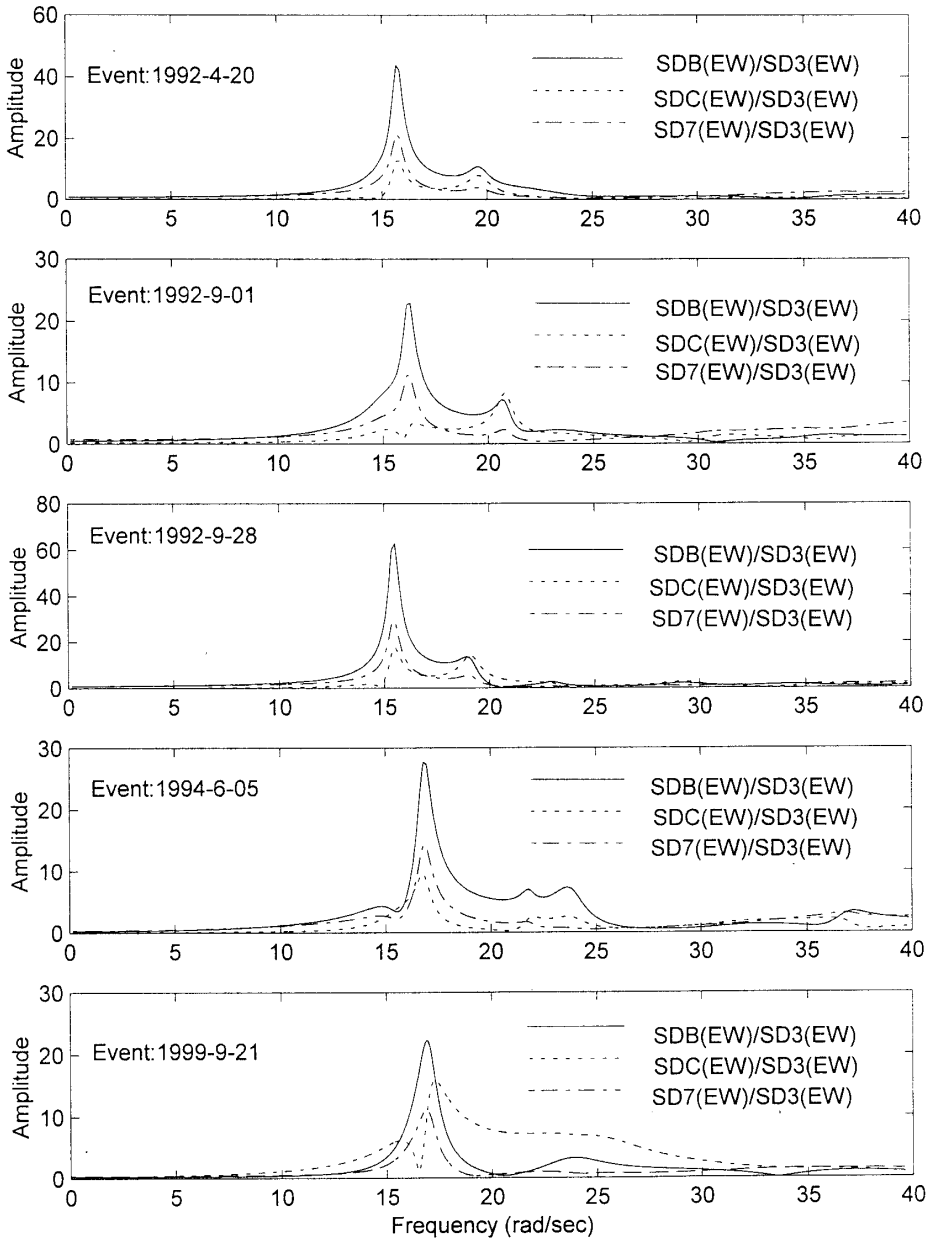


Fig. 9. Comparison on the identified $H(SDB:EW/SD3:EW)$, $H(SDC:EW/SD3:EW)$, and $H(SD7:EW/SD3:EW)$ from different seismic events.

from ARX model. As the response of dam excited by shaker force was kept at a very low level, thus the response data were easily contaminated by ambient noise.

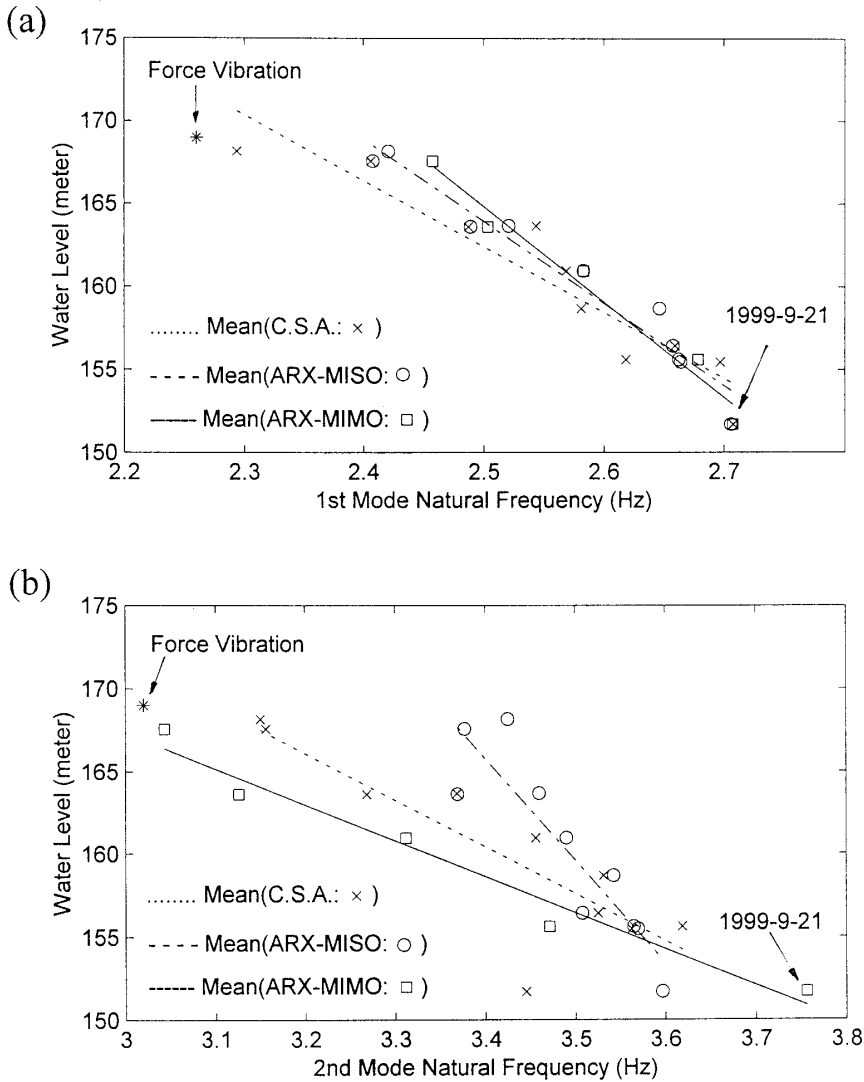


Fig. 10. Plot of the estimated modal frequencies with respect to the height of water level in the reservoir (a) first mode, (b) second mode.

(5) The relationship of identified damping ratio with respect to natural frequency was shown in Fig. 11. The first mode damping ratio identified from ARX(MISO) model are near to 2.5% for all natural frequency; the first mode damping ratio from the ARX(MIMO) model increases with the natural frequency increases. The second mode damping ratio of ARX(MISO) model distribute over a large range (about 3–8%); but the results of ARX(MIMO) model are near to a constant (about 2%) under the low level seismic excitation, the damping ratio

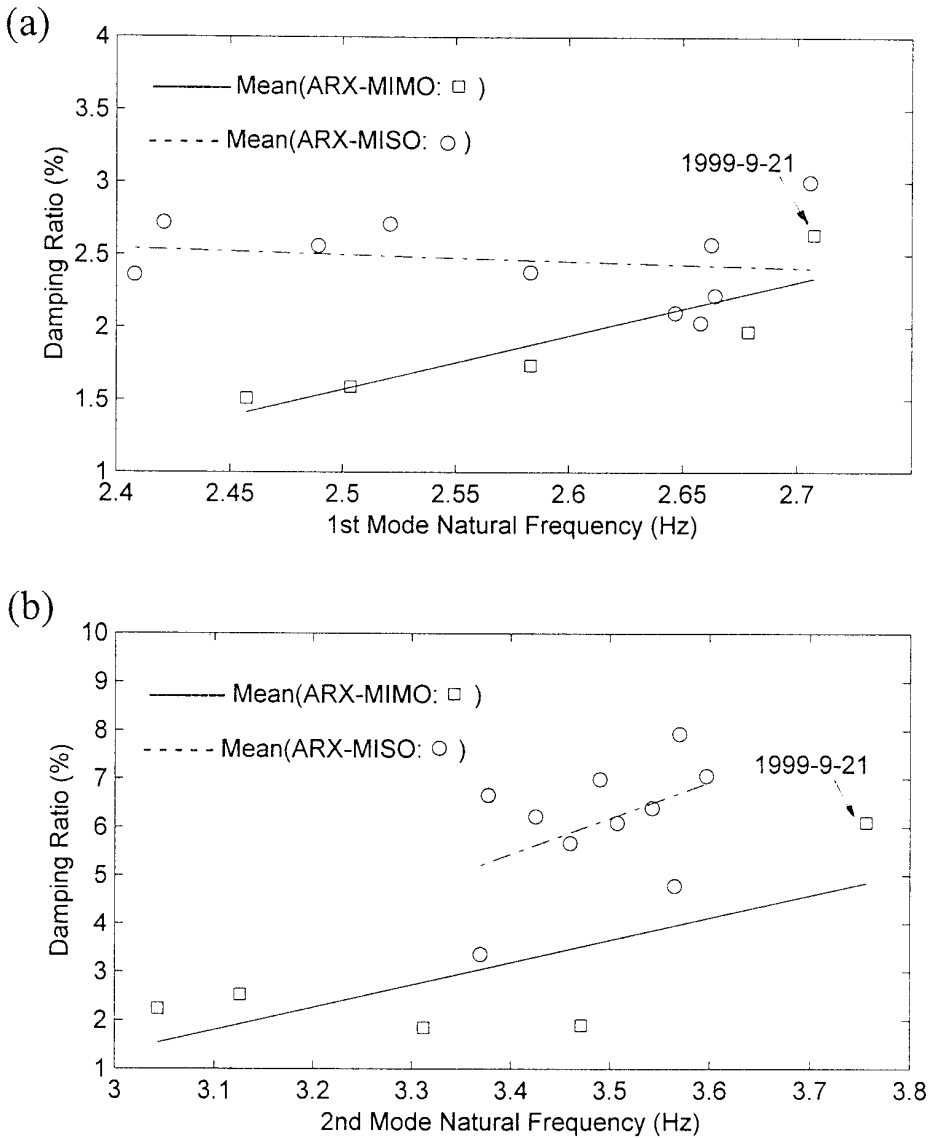


Fig. 11. Plot of the estimated modal damping ratios with respect to the estimated modal frequencies (a) first mode, (b) second mode.

value is abruptly increased under strong ground motion excitation (for Chi-Chi earthquake, the identified damping ratio is high to 6.1%), the relationship of the damping ratio with natural frequency was not a linear. Based on the above study, the bias error between the regression line and the identified damping ratio is much smaller for the ARX(MIMO) model. It is believed that the ARX(MIMO) model results looks more reasonable.

5. Spatial Variation of Free-Field Motion

Because of the large size of the dam body, there exist the spatial variation of seismic motion along the dam foundation interface due to the travelling of waves. Spatial variation along the interface also results from scattering the waves due to the canyon geometry. Motion at the surface of the canyon is found to depend on the canyon-width-to-wave-length ratio, wave incident angle, and wave type. In general, motions near the upper corner of the canyon facing the incident wave are amplified. Thus using a uniform motion at the interface may result in errors in the dam response prediction. This is the reason that multiple inputs identification algorithm was used to identify the dynamic characteristics of the dam during earthquake. Since the strong motion array of Fei-Tsui dam had six accelerometers at the free canyon surface, it is possible to analyse the spatial variation of ground motion along the canyon surface.

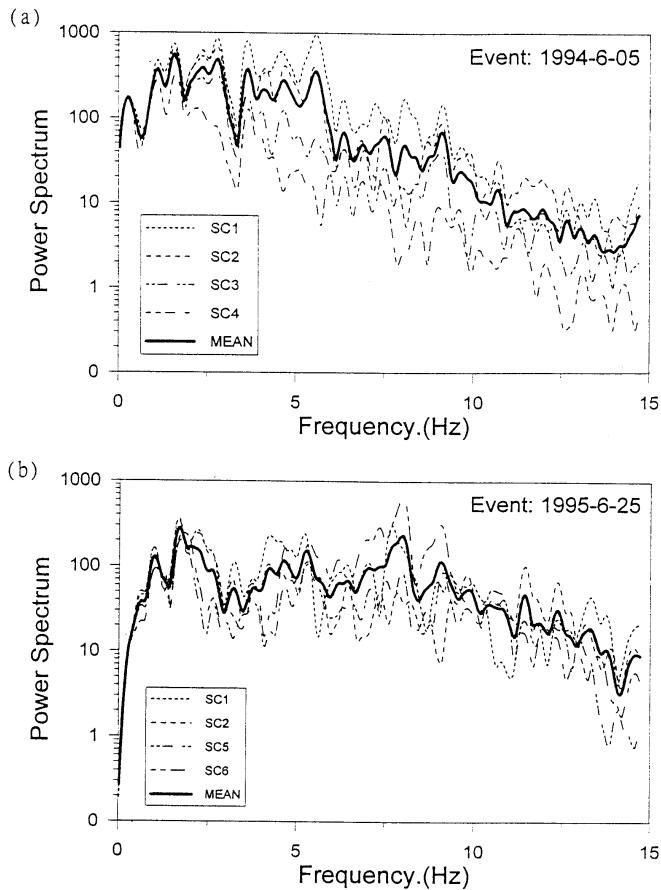


Fig. 12. Power spectrum of recorded acceleration along the canyon free-field stations for: (a) event 1994-6-05, (b) event 1995-6-25.

From the recorded ground motion along the canyon surface, Fig. 12 shows the power spectrum of free-field ground motion from two seismic events. It is found that the high frequency signals decay faster for 1994-6-5 event (depth = 5.3 km, epicenter distance = 43 km) than 1995-6-25 event (depth = 39.9 km, epicenter distance = 34 km). It means that the earthquake with shallow focal depth high frequency signals may decay faster. The coherence function of the recorded accelerations along the canyon for the above two seismic events is examined. Figure 13 shows that incoherence was observed between one station with the other station. This means that nonuniform input ground motions for the arch dam during earthquake excitation is obvious.

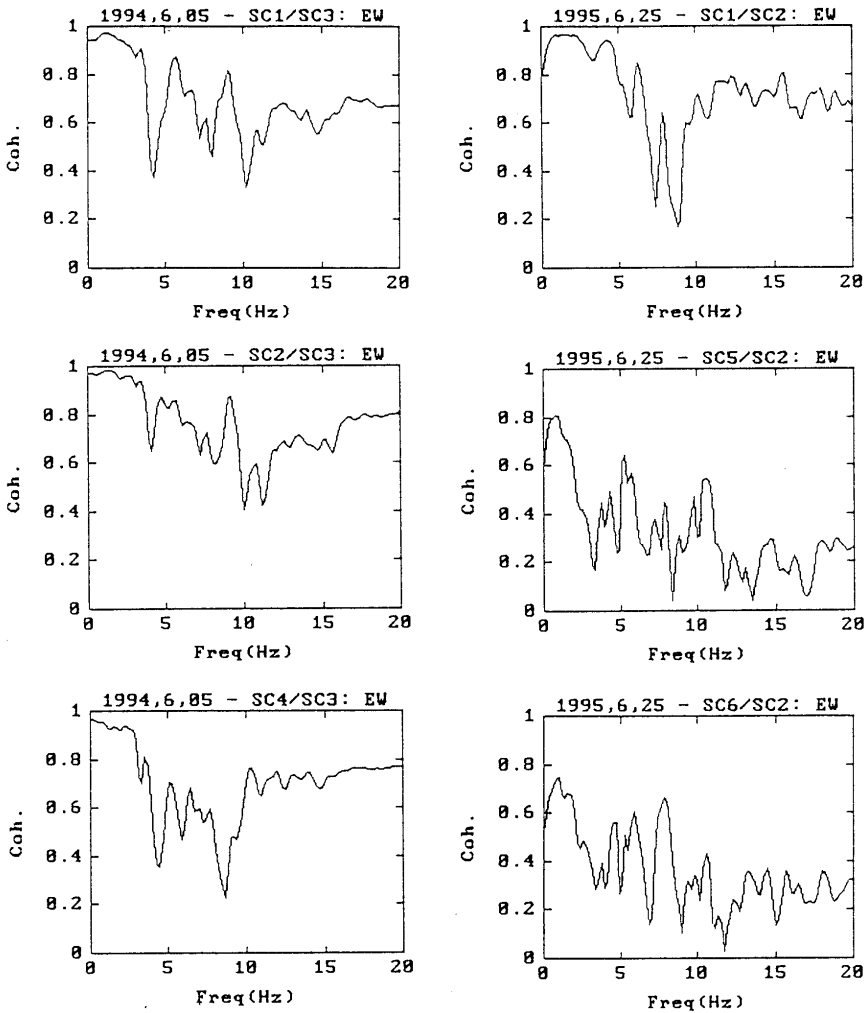


Fig. 13. Plot of coherence function of the east-west direction recorded motion along the canyon free-field (a) Event 1994-6-05, (b) Event 1995-6-25.

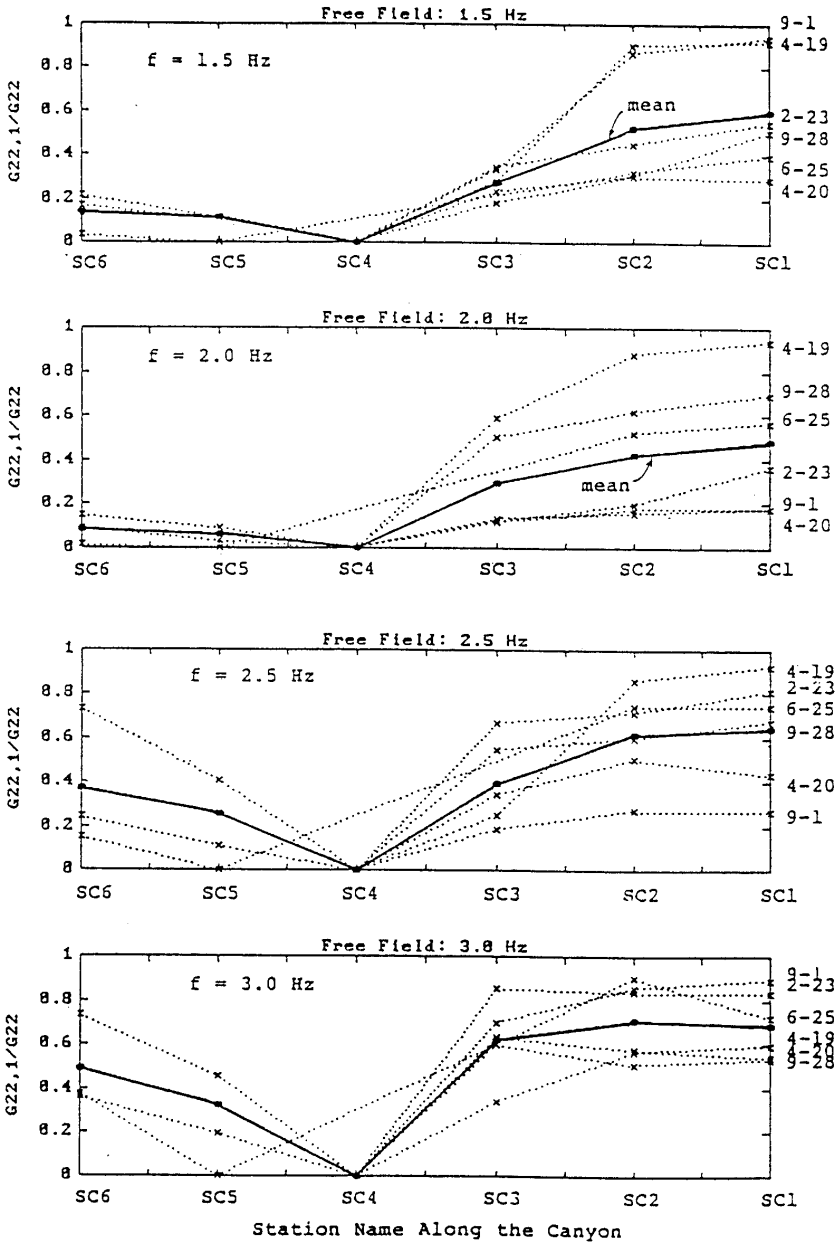


Fig. 14. Observation on the loss of coherence ($G_{22,1}/G_{22}$) along the free-field stations at frequency 1.5, 2.0, 2.5, 3.0 Hz.

In order to further understand that the coherence of canyon surface motion with respect to the motion at the bottom of canyon (consider the station SC4 as a reference station) is also studied. The loss of coherence, defined as¹⁵

$$\tilde{\gamma}_{12}^2 = 1 - \gamma_{12}^2(f) = 1 - \frac{G_{22:1}}{G_{22}} \quad (27)$$

where the superscript “2” the output signal (i.e. the motion of reference station SC4) and “1” the input signal (the canyon surface motion). Here consider the power spectrum of output G_{22} can be decomposed into two parts, one is coherent output spectrum $G_{22:1}$ and the other one is the noise output spectrum $G_{22,1}$. The smaller value of $G_{22,1}/G_{22}$ the stronger coherence between “2” and “1”, become obvious. Figure 14 shows the loss of coherence along the canyon surface with respect to the reference station (i.e. station SC4) at frequency 1.5 Hz, 2 Hz, 2.5 Hz and 3 Hz. From this figure, it is found that the coherence decreases with the increases of spatial distance at all frequencies.

6. Conclusions

The main purpose of this paper is to use the identificaion techniques to study the dynamic characteristics of the arch dam from the force vibration test data and its seismic data. The following conclusions are made:

- (1) Before the seismic event occurred, the preearthquake seismic evaluation can be performed by the forced vibration test. The natural frequencies, damping ratio and mode shape can be identified from the forced vibration data. These test data, identified parameters and mode shapes can be stored as basic reference data for further seismic safety evaluation.
- (2) The multiple input/multiple outputs discrete time ARX model is used to identify the modal frequencies, damping ratios and frequency response functions of the dam. The multiple inputs ARX model is employed to consider the nonuniform inputs from the abutment of the arch dam. The multiple outputs ARX model is necessary to describe the global behavior of the dam. To verify the accuracy of the identification result, through conditioned spectral analysis the multivariable ARX model proves to be an accurate method in the identification of dynamic characteristics.
- (3) The estimated frequency response function between longitudinal input motion (SD3:NS) and the transverse output motion (SDB:EW) is one of important frequency response function because of the large amplitude in it. This means that the contribution of the north–south direction input motion of the abutment to the east–west direction output motion cannot be omitted.
- (4) The identified first two modal frequencies of the system decreases with the increases in the dam reservoir water level. This can be explained as the effect of added mass from water pressure. The identified damping ratio from the strong motion input (Chi-Chi earthquake) was greater than the results of low level excitation. The bias error between regression line and the identified damping ratio is much smaller for the ARX(MIMO) model. It is believed that identified results from the ARX(MIMO) model looks more reasonable.

- (5) The identified system parametric model can provide the postearthquake safe evaluation of the dam. By selecting a suitable system model, and subjected to the excitation of current earthquake from the abutment, one can predict the seismic response of the dam. A comparison between the predicted response and recorded dam response can be checked if there are abrupt changes then safety evaluation and inspection on the dam body can be made.

Acknowledgements

The authors wish to express their thanks to Bureau of Fei-Tsui Dam, Taipei City Government for the support on this research project. The support from National Center for Research on Earthquake Engineering (NCREE) on the forced vibration test is also acknowledged.

References

- Abdel-Ghaffar, A. M. and Scott, R. F. [1981] "Vibration test of full-scale earth dam," *J. Geotech. Engrg. Div. ASCE*, **107**, GT3, 241–269.
- Bendat, J. S., Palo, P. A., Coppolino, P. N. [1982] "A general identification technique for nonlinear differential equation of motion," *Probabilistic Engrg. Mech.* **7**, 1992, 43–61.
- Bendat, J. S. and Piersol, A. G., [1986] *Earthq. Engrg. Struct. Dyn.* 2nd Edition, John Wiley & Sons, Inc.
- Clough, R. W., *et al.*, [1984] "Dynamic response behaviour of Quan Shui Dam," Earthquake Engineering Research Institute, *Research Report No. UCB/EERC-84/20*, University of California, Berkeley.
- Dinum, P. J., Dungar, R., Ellis, B. R., Jeary, A. P., Reed, G. A. L., Severn, R. T. [1982] "Vibration tests on Emosson arch dam, Switzerland," *Earthq. Engrg. Struct. Dyn.* **10**, 447–470.
- Duron, Z. H. and Hall, J. F., [1986] "New techniques in forced vibration testing," *Recent Advances in Structural Dynamics*, ed. G. C. Pardo, ASCE, 16–33.
- Ghanem, R. G., Gravin, H., Shnozuka, M. [1991] "Experimental verification of a number of structural system identification algorithm," *Technical Report NCEER-91-0024*.
- Housner, J. B. and Jennings, P. C. [1969] "Modal interference in vibration test," *ASCE, J. Engrg. Mech. Div.* **95**(EM4), 827–839.
- Ljung and Lennart, [1987] *System Identification: Theory for the User*, Prentice-Hall Inc., New Jersey.
- Loh, C. H. and Tou, I. C. [1995] "A system identification approach to the detection of changes in both linear and non-linear structural parameters," *Earthq. Engrg. Struct. Dyn.* **24**, 85–97.
- Loh, C. H. and Wu, T. S. "Identification of Fei-Tsui arch dam from ambient and seismic response data," *Soil Dyn. Earthq. Engrg.* **15**, 465–483.
- Mau, S. T. and Ghia, J., [1988] "Arch dam system identification using frequency response test data and nonclassical modes," *Proceedings of 9WCEE*, Tokyo-Kyoto, Japan, VI, 379–384.
- Mau, S. T. and Wang, S. [1989] "Arch dam system identification using vibration test data," *Earthq. Engrg. Struct. Dyn.* **18**, 491–505.
- Park, I. W. and Ma, K. F. "Characteristic of model coupling in nonclassical damped systems under harmonic excitations," *J. Applied Mechanics, ASME*, 61/77.

- Safak, E. [1989a] "Adaptive modeling, identification and control of dynamic structural system, I: Theory," *ASCE, J. Engrg. Mech.* **115**, 2386–2405.
- Safak, E. [1989b] "Adaptive modeling, identification and control of dynamic structural system, II: Application," *ASCE, J. Engrg. Mech.* **115**, 2406–2426.